F. San José Martínez
F.J. Muñoz
F.J. Caniego
F. Peregrina

Morphological Functions to Quantify Three-Dimensional Tomograms of Macropore Structure in a Vineyard Soil with Two Different Management Regimes

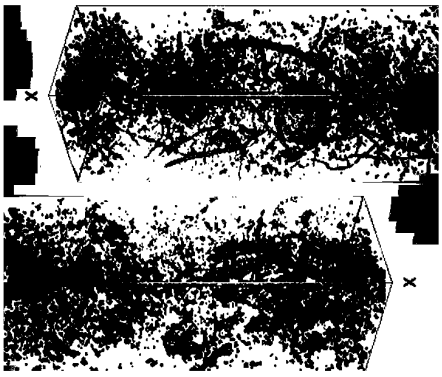

Soil tomography and morphological functions built over Minkowski functionals were used to describe the impact on pore structure of two soil management practices in a Mediterranean vineyard.

Soil structure controls important physical and biological processes in soil–plant–microbial systems. Those processes are dominated by the geometry of soil pore structure, and a correct model of this geometry is critical for understanding them. Soil tomography has been shown to provide rich three-dimensional digital information on soil pore geometry. Recently, mathematical morphological techniques have been proposed as powerful tools to analyze and quantify the geometrical features of porous media. Minkowski functionals and morphological functions built over Minkowski functionals provide computationally efficient means to measure four fundamental geometrical features of three-dimensional geometrical objects, that is, volume, boundary surface, mean boundary surface curvature, and connectivity. We used the threshold and the dilation and erosion of three-dimensional images to generate morphological functions and explore the evolution of Minkowski functionals as the threshold and as the degree of dilation and erosion changes. We analyzed the three-dimensional geometry of soil pore space with X-ray computed tomography of intact soil columns from a Spanish Mediterranean vineyard by using two different management practices (conventional tillage versus permanent cover crop of resident vegetation). Our results suggested that morphological functions built over Minkowski functionals provide promising tools to characterize soil macropore structure and that the evolution of morphological features with dilation and erosion is more informative as an indicator of structure than moving threshold for both soil managements studied.

The spatial arrangement of soil constituents—usually referred to as soil structure—controls important physical and biological processes in soil–plant–microbial systems, where microbial population dynamics, nutrient cycling, diffusion, mass flow, and nutrient uptake by roots take place across many orders of magnitude of length scale (Young and Crawford, 2004). Natural soils display a highly heterogeneous and complex structure that involves a wide range of scales from rough surfaces of particles, complex pore space geometries, and intricate networks of cracks to the extremely wide variation of the soil horizons boundary. Nevertheless, the description of flow and transport phenomena in soil addresses critical problems of soil functioning and ecosystem processes. However, the mismatch of scales is a persistence theme. For example, environmental contamination due to agricultural activities take place on the scale of several meters, while the controlling physical mechanisms based on capillarity forces are in the range of microns (Lehmann et al., 2008). As it is often impossible to measure and model at the scale of interest, flow and transport on the unsaturated zone is analyzed at the Darcy scale, under the assumption of the homogeneity that natural soils do not have. A correct model of this geometry is critical for understanding flow and transport processes in soils, creating synthetic soil pore space for hypothesis and model testing, and evaluating similarity of pore spaces of different soils (Dullien, 1992).

Indirect methods are often used to determine the distribution of pores sizes as a part of assessing geometry of soil pore structure. When solid phase is considered as the complementary phase of soil pore space, particle size distributions or water retention curves are used to infer pore properties. But this approach has serious shortcomings. The same distribution of particles sizes determines different pore structures. These different structures

will confer different hydraulic properties due to the fact that pore connectivity plays a major role on flow and transport phenomena (Vogel and Roth, 2001).

New technologies, both in the realm of image acquisition of soil structure and numerical simulation of processes on complex geometrical structures like lattice Boltzmann methods (Sukop and Thorne, 2007), have opened new avenues to this old standing problem. It has being suggested that these techniques would provide a better understanding of the linkage between structure and flow and transport processes in natural soils and in this way they would improve the predictability of this models in the vadose zone (Lehmann et al., 2008). Mathematical morphology has been applied successfully to the description of pore space geometry, and some recent results (Lehmann, 2005; Mecke and Arns, 2005; Schlüter and Vögel, 2011) on the linkage of geometrical features and flow parameters (i.e., structure and functioning) represent a promising advance in using this path.

X-ray computed tomography provides a direct methodology to use three-dimensional information to quantify geometrical features of soil pore space (Peyton et al., 1994; Perret et al., 1999; Pierret et al., 2002; Mees et al., 2003, Lehmann et al., 2006). In the last few decades this rich three-dimensional geometrical information has begun to be analyzed with the mathematical tools of the mathematical morphology (Mecke and Stoyan, 2000, 2002; Banhart, 2008)

Mathematical morphology (Serra, 1982) as a mathematical theory combines a number of mathematical techniques aimed at quantifying geometrical features of geometrical objects. These mathematical techniques belong to well-established mathematical fields as integral geometry (Santaló, 1976), stochastic geometry (Matheron, 1975), or digital topology and geometry (Klette and Rosenfeld, 2004). Dullien and collaborators (see Dullien, 1992 and the references therein) used these techniques to investigate the relationship between soil pore structure and fluid transport phenomena. At that time they mostly used stereology to gain three-dimensional information from two-dimensional images obtained by image analysis of soil sections. See also Moran et al. (1989, 1990), Vogel and Kretzschmar (1996), Vogel et al. (2005), or Horgan (1998), to name a few.

Minkowski functionals provide computationally efficient means to measure four fundamental geometrical properties of three-dimensional ~~geometrical~~ objects such as pore space. The properties are the volume, the boundary surface, the mean boundary surface curvature, and the connectivity of the object of interest. The Hadwiger's theorem (Santaló, 1976) states that any functional that assigns a number to any three-dimensional object and meets some geometrical restrictions is a linear combination of the Minkowski functionals. Therefore, these functionals provide a powerful tool to describe quantitatively the three-dimensional geometry. Mecke (1998) and Roth et al. (2005) make use of Minkowski functions based on threshold variation of Minkowski functionals to characterize two-dimensional porous structures. Also, two-dimensional porous structures were investigated by Mecke (2002) and Vogel et al. (2005) with Minkowski functions based on dilations and erosions. Arns et al. (2002, 2004) considered the evolution of Minkowski functionals with dilations and erosions to characterize three-dimensional images of Fontainebleau sandstone.

We used morphological functions built over Minkowski functionals to analyze soil structure through the investigation of the geometry of soil pore space with three-dimensional images from X-ray computed tomography of intact soil columns from a Mediterranean vineyard with two different soil management practices [conventional tillage management (CTM) versus permanent cover crop (PCC) of resident vegetation]. The research was based on Minkowski functional application to results of changes of image threshold and morphological transformations of erosion and dilation.

Morphology of Soil Pore Space

Morphological Operations

The basic morphological operations are dilation and erosion. Grains or pore space in a three-dimensional CT image can be idealized as sets of points in three-dimensional space. These types of geometrical objects will be the mathematical objects of interest. Mathematically, an object is a closed and bounded set. A ball is a closed set if this ball contains the points of the spherical surface that define the ball—its boundary. And it is a bounded set because it is contained in a sphere of finite radius. Dilation of an object expands it. This new object can be thought of as being the union of all balls with a given radius r centered at points of the original object. If the original object is a ball of radius r_0, the dilated object by balls of radius r will be a new ball of radius $r_0 + r$.

We consider a generic object K and a ball B of radius one in which its center is located at the origin of coordinates. Both K and B are objects, closed and bounded sets, but K is the object of interest or simply an object that we scrutinize with the object B that is called structuring element. A ball of radius r centered at the origin, rB, is obtained by multiplying the points of B by r. A ball of radius one centered at point $\mathbf{x}$, $B_{\mathbf{x}}$, is obtained by adding x to every point of B. Scalar multiplication by a number r produces an expansion with scaling factor r when $r > 1$ and a contraction with scaling factor r when $r < 1$. Addition with a vector $\mathbf{x}$ produces a translation in the direction of the vector $\mathbf{x}$ at a distance equal to the "length" of this vector—its modulus. Then, we have the following expressions that define the sets rB and $B_{\mathbf{x}}$:

$$rB = \{r\mathbf{y} : \mathbf{y} \in B\} \text{ and } B_{\mathbf{x}} = \{\mathbf{y} + \mathbf{x} : \mathbf{y} \in B\}$$

Here, rB is the set of points $r\mathbf{y}$ when y belongs to B and, $B_{\mathbf{x}}$ is the set of points $\mathbf{y} + \mathbf{x}$ when $\mathbf{y}$ belongs to B. In these expressions $r\mathbf{y}$ stands for the scalar multiplication of the scalar r and the vector $\mathbf{y}$ and $\mathbf{y}$

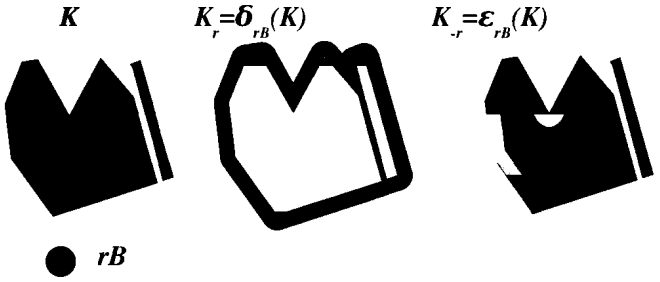

Fig. 1. Effect of dilation $K_r = \delta_{rB}(K)$ (gray plus black) and erosion $K_{-r} = \varepsilon_{rB}(K)$ (black) of object K by the structuring element rB.

+ $\mathbf{x}$ represents the sum of two vectors, $\mathbf{y}$ and $\mathbf{x}$. Thus, the dilation (Fig. 1) of the object K by balls of radius r, that is, the union of all balls $rB_{\mathbf{x}}$ of radius r centered at points $\mathbf{x}$ of K, will be another object K_r defined as

$$K_r = \cup_{\mathbf{x}\in K} rB_{\mathbf{x}}$$

In general, the structuring element could be any set that may or may not contain the origin of coordinates. Then, one has $\delta_E(K)$, the dilated set of the object K by structuring element E. In most cases it is appropriate to consider a structuring element that contains the origin of coordinates and is symmetric with respect to it: like balls centered at the origin. In this case it is verified that

$$K_r = \delta_{rB}(K)$$

The set K_r is also called the parallel body of K at a distance r or r-parallel body to K. This is the set of all points within a distance smaller than r from the object K. In this work, the structuring element will be a ball centered at the origin. Then, the dilation of an object by a ball of radius r is equivalent to the r-parallel body to K. Roughly speaking, it is like a "skin" of thickness r is added to K.

We will analyze two-colored images (black and white images) or binary images of soil. They contain two complementary phases: the phase of voids (pores) and the phase of soil matrix (mineral particles). In this case the pore space is the object of interest, and it will be black while mineral particles will form the background and it will be white as it is customary in image analysis. Then, the erosion of one phase is equivalent to the dilation of the complementary phase. Erosion of the pore space is dilation of the soil matrix, and erosion of the soil matrix is dilation of the pore space. Usually, a CT image of soil will be shown as a set of points of a cube, S, where each point is a part of pore space, P, or a part of soil matrix, M. These points are the pixels of a two-dimensional image or the voxels of a three-dimensional one. In mathematical terms,

$$S = P \cup M,\ P^c = M, \text{ and } M^c = P.$$

Here P^c represents the complementary of P, that is, the set of points in S that are not in P. These mathematical expressions indicate that the complementary set of the pore space in the cube S is the soil matrix and vice versa. Then, the erosion of an object K by a ball of radius r centered at the origin is defined as

$$\varepsilon_{rB}(K) = \left[\delta_{rB}\left(K^c\right)\right]^c$$

A more intuitive expression is given by

$$\varepsilon_{rB}(K) = \{x : rB_{\mathbf{x}} \subset K\}$$

Consequently, the erosion of an object K by a ball rB corresponds to the set of all positions of their centers within K where the structuring element rB fits completely into K (Fig. 1).

Therefore, we may generalize the notion of parallel body as follows

$$K_r = \begin{cases} \delta_{rB}(K), & r > 0 \\ \varepsilon_{rB}(K), & r < 0 \end{cases}$$

(Arns et al., 2002). Then, K_0 coincides with the original object K.

Measurements: Minkowski Functionals

Minkowski functionals are a complete set of geometrical features as established by Hadwiger's theorem (Serra, 1982). A class of objects to which Hadwiger's theorem applies is the class of sets that can be viewed as the union of a finite number of convex objects. An object K is convex when it contains any point of the segment that joins two of its points. The class of objects made up of convex objects is a very important class because any three-dimensional binary image is a set of voxels (the three-dimensional counterpart of a pixel). Voxels may be thought of as being cubes; therefore, any geometrical structure of interest in a binary image is a finite union of convex objects, or voxels. There are three geometrical conditions that a functional to which Hadwiger's theorem applies must meet. The first one is motion invariance: the number assigned by a functional must be independent of the position of the object in space when the object is translated or rotated. The second one is C-additivity:

$$\mathcal{F}(K_1 \cup K_2) = \mathcal{F}(K_1) + \mathcal{F}(K_2) - \mathcal{F}(K_1 \cap K_2)$$

That is to say, the number assigned by a functional $\mathcal{F}$ to the union of two objects K_1 and k_2 equals the value of the functionals over those two objects minus parts counted twice. And the third condition is continuity. Consider a sequence of objects $\{K_n\}$ that

approaches the object K as n tends to infinity. An example of this is the sequence of r-parallel bodies of an object K; it is clear that the sequence of r-parallel bodies $\{K_n\}$ with $r = 1/n$ approaches K as n goes to infinity or, equivalently, as r goes to zero. Then, the continuity condition is fulfilled if $\mathcal{F}(K_n)$ tends to $\mathcal{F}(K)$ as n goes to infinity. Under these conditions there are $d + 1$ numbers c_i such that

$$\mathcal{F}(K)=\sum_{i=0}^{d} c_i W_i^{(d)}(K)$$

when K belongs to the d-dimensional linear space. In this expression $W_i^{(d)}(K)$ are the Minkowski functionals that assign to any object a number. They are $d + 1$ functionals in dimension d. There are three Minkowski functionals in the plane and four in space. In the plane (the two-dimensional linear space), one has

$$W_0^{(2)}(K)=A(K),\ W_1^{(2)}(K)=L(K),\ \text{and}\ W_2^{(2)}(K)=A(B)$$

In this expression A stands for the area and L stands for the length of the perimeter of the square K. Here B is the ball centered at the origin with radius one. In space (the three-dimensional linear space), one has

$$W_0^{(3)}(K)=V(K),\ W_1^{(3)}(K)=\frac{1}{3}S(K),\ W_2^{(3)}(K)=\frac{1}{3}M(K),$$

and $W_3^{(3)}(K)=V(B)$

Here B is the ball centered at the origin with radius one, as before, V stands for the volume, S for the area of the boundary, and M for the mean breadth multiplied by 2π [it can be shown that the mean breadth of a cube of edge a is $3a/2$ (Santaló, 1976)]. When the boundary surface of K is smooth, M also represents its mean curvature (Ohser and Mücklich, 2000). Points on the boundary surface of an object with positive curvatures settle on convex parts (protrusions) of the object while points with negatives curvatures belong to concave parts (hollows) of the object. For convex objects, M is positive. Then, M can be thought of as measure of the convexity of the object or the "complexity" of its boundary.

Two ideas are worth to note here in connection with Minkowski functionals. On the one hand, they are easily computed (Michielsen and De Raedt 2001). Taking into account the C-additivity property and the fact that three-dimensional images are sets of voxels, their computation reduces to the computation of the Minkowski functionals on cubes (or voxels) and their intersections (vertices, edges, and faces). On the other hand, the Minkowski functional $W_d^{(d)}$ is the Euler-Poincaré characteristic of the object multiplied by the volume of the d-dimensional ball of radius one. In the plane one has $W_2^{(2)}(K)=\pi\chi(K)$ and $W_3^{(3)}(K)=(4\pi/3)\chi(K)$ in space. In these expressions $\chi(K)$ is the Euler-Poincaré characteristic of K. When the object of interest K corresponds to the pore space P, the Euler-Poincaré characteristic $\chi(P)$ is an index of the topology of the pore phase and it quantifies pore connectivity (Vogel and Kretzschmar, 1996). On the plane, Euler-Poincaré can be computed subtracting the number of holes of the object, $H(K)$, from the number of connected components, $CC(K)$ (Mecke, 1998):

$$\chi(K)=CC(K)-H(K)$$

In this context a connected component of an object is any part of it whose points are connected to one another by curves of points contained in the object. Then, a disk has Euler-Poincaré characteristic equal to one because it has one connected component and no holes. A punctured disk has Euler-Poincaré number equal to zero; a disk punctured twice, minus one, and so on. If the object is just the union of n separated grains on an image, the Euler-Poincaré characteristic equals n. This object has n connected components. Similar definitions and relations hold in space though distinction between two kinds of holes must be made. In space, the Euler-Poincaré characteristic can be computed as the sum of the number of connected components, $CC(K)$, and the number of cavities of the object, $C(K)$, subtracted by the number of tunnels, $T(K)$ (Mecke, 1998):

$$\chi(K)=CC(K)-T(K)+C(K)$$

Cavities are holes completely surrounded by the object, while tunnels are holes through the object connected with the exterior or background. If the object is just a separate union of n grains of an image, the Euler-Poincaré characteristic equals n. Then, a solid ball has a Euler-Poincaré characteristic equal to one, a ball with a cavity in it, two, a ball with two cavities, three, and so on. However, if the ball has a tunnel that goes through it, the Euler-Poincaré characteristic is zero, two tunnels gives a Euler-Poincaré characteristic equal to minus one, and so on.

Describing Objects by Functions

Mathematical morphology offers a powerful description of objects in terms of functions. This technique is similar to the process that provides particle size distributions by morphological analysis of soil images (Serra, 1982; Soille, 2002; Vogel, 2002).

Consider a three-dimensional binary image of soil where the void phase K is the object of interest. Let K_r be, as before, the dilation of K by balls of radius r when $r > 0$ and the erosion of K by balls of radius r when $r < 0$. Then, consider any Minkowski functional, say M, and the function

$$f(r)=M(K_r)$$

This family of functions built over the Minkowski functionals provides a way to investigate the morphology of the pore space K as it is dilated and eroded with balls of increasing radius r. Vogel et al. (2005) used this approach on two-dimensional images to describe crack dynamics in clay soil. Roth et al. (2005) make use of opening (i.e., erosion followed by dilation) to build Minkowski functions to quantify permafrost patterns with aerial photographs. This family of functions adds new information to that provided by Minkowski functionals as they yield the pore size distribution of the porous structure. Arns et al. (2004) characterize disordered systems and match model reconstructions to three-dimensional images of Fontainebleau sandstone with Minkowski functions based on dilations and erosions. Vogel et al. (2010) take advantage of Minkowski functions based on openings to quantify soil structure of arable soil and of repacked sand using three-dimensional images from X-ray tomography of samples of different sizes recorded at different resolutions.

Mecke (1996) consider a different type of Minkowski function. In this case the original two-dimensional image is a grayscale image before segmentation. A series of binary images are obtained when the threshold varies from the minimum value of the grayscale to its maximum. Minkowski functionals are evaluated on each binarized image of the series, and four Minkowski functions are defined when the Minkowski functionals evolve as a function of threshold. Roth et al. (2005) also made use of this type of function to quantify permafrost patterns obtained from aerial two-dimensional photographs. It is widely recognized that thresholding is a fairly subjective operation and there is no generally accepted procedure for image segmentation, even in the soil science community. Nonetheless, this type of function based on threshold variations allows examining raw data and provide a way to analyze patterns before loss of information produced when segmentation is performed.

We investigated in a three-dimensional setting how Minkowski functions based on the variation of the threshold of grayscale three-dimensional images and Minkowski functions based on dilations and erosions of segmented three-dimensional images can be used to characterize soil pore structure of cultivated soil. We made use of X-ray computed tomography for soil columns imaging.

Soil Samples

Site Description and Sample Collection

The columns were collected at the experimental farm "Finca La Grajera," property of La Rioja region government (northern Spain) (42°26′34″18 N lat.; 2°30′53″07 W long.), on December 2010. The field slope is about 10.2% with west–east orientation. The soil is classified as fine-loamy, mixed, thermic Typic Haploxerepts according to the USDA soil classification and contained 230 g kg^{-1} clay, 433 g kg^{-1} silt, 337 g kg^{-1} sand, 9.3 g kg^{-1} organic matter, and 149 g kg^{-1} carbonates, with pH 8.62 and electrical conductivity 0.17dS m^{-1} at the Ap horizon (0–20 cm). Climate in the area is semiarid according to the UNESCO aridity index (UNESCO, 1979), with heavy winter rains and summer drought conditions. For the period 2005 to 2009, the average annual precipitation was 470 mm, average annual temperature was 13°C, and average annual potential evapotranspiration (FAO–Penman) was 1132 mm.

In this study we selected four columns collected between rows of the vineyard that was established in 1996 with *Vitis vinifera* L. 'Tempranillo,' grafted on 110-R rootstock. Two types of soil cover management in between rows were undertaken: CTM between rows, which consisted of soil tillage at 15 cm depth by cultivator once every 4 to 6 wk as required for weed control during the grapevine growth cycle, and PCC of resident vegetation, which was dominated by annual grass and forbs common to La Rioja vineyards [see Peregrina et al. (2010) for more details]. Columns were extracted vertically by percussion drilling between rows, within PVC cylinders of 7.5 cm interior diameter and 30 cm height from the upmost part of soil profile.

Soil Tomography: Image Acquisition, Filtering, and Thresholding

Soil columns were scanned with a PerkinElmer amorphous silicon (a-Si) detector with 2048 by 2048 pixels and a Feinfocus FXE 225.51 microfocus beam source tube. It was operated at 190 kV (53 uA) acceleration voltage and 20 W target power, and the tube had a tungsten target installed. In addition, a collimator to reduce stray radiation and a 200 μm steel filter in front of the target was used. Only the upper half of the column was scanned, and the region between 8 and 15 cm was selected to have a resolution of 50 μm. In this way soil macropore structure important for intense renewal of air and serving to transport and distribute water in soil (Brewer, 1964) was imaged.

Raw data from tomography correspond to a stack of 1706 two-dimensional 16-bit grayscale images with a pixel size of 50 μm. These horizontal sections are disks of 7.5 cm diameter, 50-μm apart from one another. Thus the three-dimensional image is made up of voxels of 50 μm. They can be pictured as being situated at the center of each pixel. Light values of the grayscale designate voxels corresponding to low densities of the soil column, whereas high values indicate voxels of high density parts of the column. The original two-dimensional projections were filtered by a 3 by 3 median filter before reconstruction to reduce random noise from the detector. It is a nonlinear smoothing method to reduce isolated noise without blurring sharp edges (Wang and Lai, 2009). This kind of noise contains random occurrences of white pixels (see Fig. 2a). When performing a 3 by 3 median filter, a square neighborhood window of 3 by 3 pixels is chosen. This window is centered at each pixel of the image. Let us call this pixel the reference pixel. Then, the median of the grayscale values of the pixels of the window is evaluated. And the original value of the grayscale of the reference pixel is replaced by the median value. This operation is repeated for each pixel of the image.

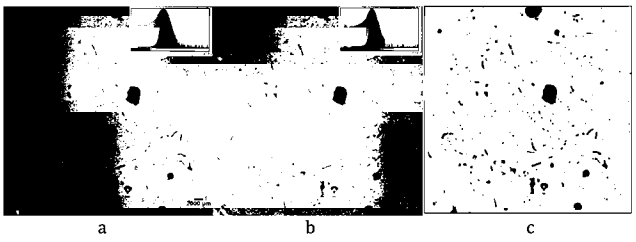

Fig. 2. Illustration of image enhancement and binarization of sample PCC1: (a) a horizontal section of 960 by 960 pixels of the original grayscale image and its histogram in the inset—the histogram is also displayed with the logarithmic scale in the vertical axes to visualize the two maxima; (b) enhancement of that section with a 3 by 3 median filter and its histogram in the inset—it is also represented with logarithmic scale in the vertical axes, and it is worth noting that the two maxima are more marked here than in the original grayscale image (Fig. 2a); and (c) binarized image of the previous section where black corresponds to voids.

The segmentation process provides a way to separate the object of interest from the background, in this case the pore space from the soil matrix. This process produces binary images when a threshold is selected and every voxel with a grayscale value lower than the selected threshold is considered as part of the pore space and set to 1 (black), while every voxel with a grayscale value higher than the selected threshold is considered as part of the soil matrix and set to 0 (white). We selected a global method (Iassonov et al., 2009) because we focused primarily on the analysis of geometrical features' evolutions as threshold varies. The modes method of thresholding was chosen to generate binary images (Sonka et al., 1998). In this procedure the histogram is iteratively smoothed until there are only two local maxima. Then, the threshold is chosen at the midpoint between these local maxima. Figure 2 illustrates image enhancement and binarization, and Fig. 3 shows the view of three-dimensional reconstruction of pore space in a binary image. Plots of histograms with logarithmic scale on the vertical axis are displayed (Fig. 2a and 2b, inset) to show the two maxima. Notice the different pore structures that display a typical sample from soil under cover crop of resident vegetation (Fig. 3a) and from soil under conventional tillage (Fig. 3b). The homogeneity of the pore space produced by tillage is obvious (Fig. 3b) as compared to the much more heterogeneous result of the resident vegetation crop (Fig. 3a).

Morphological Transformations and Measurements of Soil Pore Space

As mentioned above, two different approaches were used to explore soil macroporosity of the scanned columns. First, we used the full range of raw data to explore the complexity of pore structure at different threshold scales (Mecke, 1996; Roth et al., 2005). We investigated how Minkowski functionals evolve when the threshold varies (Mecke, 1998; Michielsen and De Raedt, 2001). Second, we considered binary images segmented with the modes method procedure. In these images, the pore space was the object of interest, while soil matrix was the background. To study pore structure, we investigated the evolution of Minkowski functionals as successive erosions and dilations when balls of increasing radius are performed on the binary images (Arns et al., 2002; Vogel et al., 2005).

We followed the procedure developed by Mecke (1996) and the code published by Michielsen and De Raedt (2001) to compute Minkowski functionals. For sake of clarity, we illustrate this procedure in two-dimensional images made up of pixels that geometrically are squares. The object of interest K is a finite union of squares (compact and convex object). Each square is considered to be decomposed into the four points of its four vertices, the four open segments of its four edges, and the rest of the square, that is, the interior of the square. The square of each pixel is the union of nine disjoint sets: four points, four open segments and the interior of the square. As a consequence, we only needed to know the Minkowski functional of these three types of sets (a point, an open segment, and an open square) and then used C-additivity extended to the union of an arbitrary amount of sets. If n_s is the number of squares of the object, n_e the number of edges, and n_v the number of vertices of the pixels of the object of interest counted once, it is easy to verify that (Michielsen and De Raedt, 2001)

$$A(K)=n_s,\ L(K)=-4n_s+2n_e, \text{ and } \chi(K)=n_s-n_e+n_v$$

For three-dimensional objects, a similar argument shows that (Michielsen and De Raedt, 2001)

$$V(K)=n_c, S(K)=-6n_c+2n_f, \pi^{-1}M(K)=3n_c-2n_f+n_e,$$

and $\chi(K)=-n_c+n_f-n_e+n_v$.

In this expression n_c is the number of cubes and n_f is the number of faces of the voxels of the object K, counted once.

Results and Discussion

Minkowski functionals were evaluated on five cubes per column. The edge length of these cubes was 340 voxels. We generated a series of 60 three-dimensional binary images from each cube c_i (i = 1...5) by choosing 30 equidistant different thresholds ρ between zero and the maximum value of the grayscale on cube c_i, and another 30 were obtained by rescaling those 30 thresholds first selected by a factor of 1/2.5 to refine the data set. As a result we had a series of pore spaces (black phase) P_ρ for each threshold ρ, and the morphological functions built over the Minkowski functionals averaged over the volume of cube c_i

$$V(P_\rho)/V(c_i),\ S(P_\rho)/V(c_i),\ M(P_\rho)/V(c_i),\ \chi(P_\rho)/V(c_i).$$

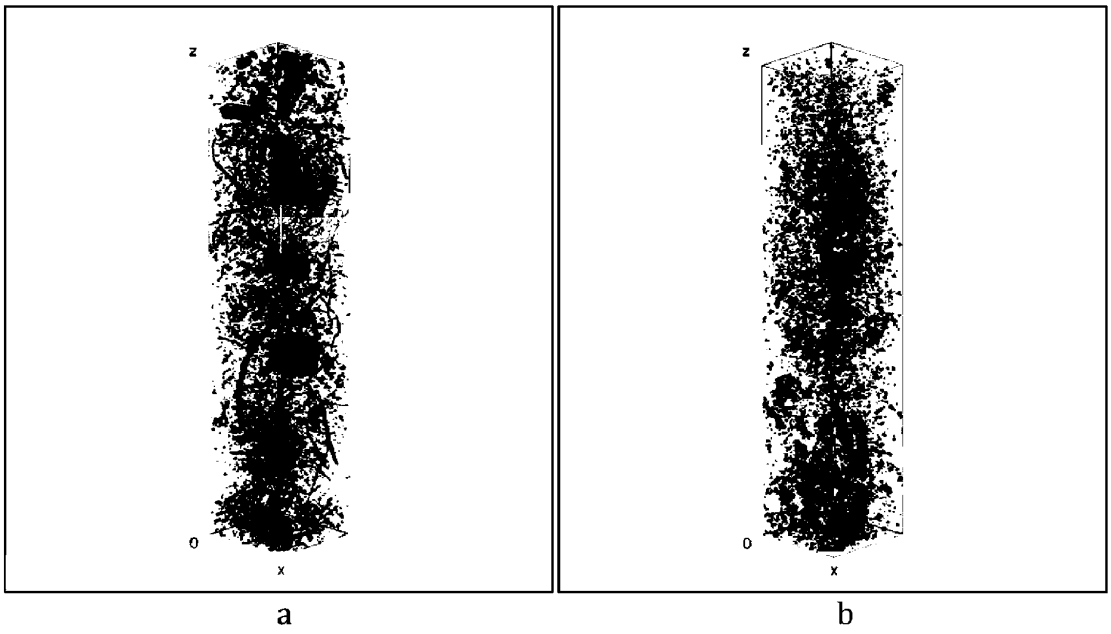

Fig. 3. View of three-dimensional reconstruction of pore space (black) of a binary image in a box that is 8.5 cm high (z axis) and 1.7 cm long (x axis) and wide (y axis): (a) sample PCC1 from natural vegetation cover and (b) sample CTM2 from tillage soil.

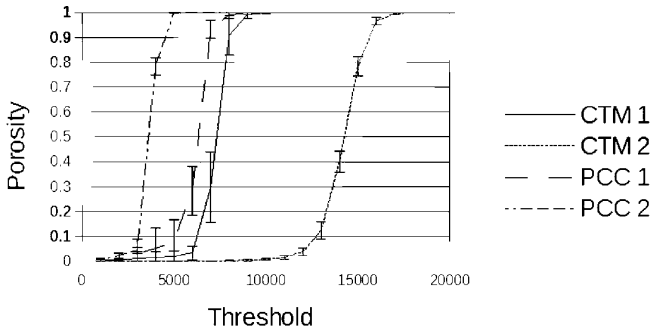

Fig. 4. Image porosity as a function of threshold.

The first density corresponded to the image porosity (i.e., the volume fraction of black voxels) of cube c_i for the threshold ρ, $\phi(\rho) = V(P_\rho)/V(c_i)$ (Fig. 4). As variables ϕ and ρ are interchangeable because $\phi(\rho)$ is an increasing function of ρ, it is possible to build the inverse function $\rho(\phi)$. Let us recall that $\phi(\rho)$ it is not the soil porosity of the cube but the volume fraction of voxels with greyscale level smaller than ρ, that is, it is the porosity of the cube if it were segmented chosen ρ as threshold. As the different images have very different mean gray values, it was much more convenient to relate the results to porosity. Moreover, the range of the threshold varied from sample to sample, while the porosity varied from zero—when the threshold was zero—to one when the threshold attained the maximum possible value of the grayscale. As a consequence, this new parameter helped the comparison of geometrical features' evolutions between different samples. Then, we had the morphological functions built over Minkowski functionals as densities when the threshold varied as function of porosity (Fig. 5)

$$\overline{S}_\rho(\phi) = S\left[P_{\rho(\phi)}\right]/V(c_i),\ \overline{M}_\rho(\phi) = M\left[P_{\rho(\phi)}\right]/V(c_i),$$

$$\overline{\chi}_\rho(\phi) = \chi\left[P_{\rho(\phi)}\right]/V(c_i).$$

This was the evolution of specific area, specific mean curvature, and specific connectivity of pore space P of cube c_i when threshold varied as a function of volume fraction or image porosity.

The binary image of each column segmented by the method of modes was analyzed, and the pore space P in cube c_i was eroded and dilated to yield the parallel body P_r, the object of interest. Let us recall that P_r is the dilation by balls of radius r of the pore space P when r is positive; alternatively, when r is negative, P_r is the erosion by balls of radius r of the pore space P. Parameter r took 19 different values for erosions and nineteen for dilation, as well. The value of r started at 0 and was incremented in steps of the voxel size (i.e., 50 microns). We chose the number of dilations and erosions to keep the execution time of the code manageable to perform morphological transformations and to evaluate Minkowski functionals on a Linux system with an Intel Core™ i3 microprocessor.

As before, we considered densities and we used image porosity (i.e., volume fraction) to parameterize them. In this case we had $\phi(r) = V(P_r)/V(c_i)$ (Fig. 6), which is an increasing function of r, and

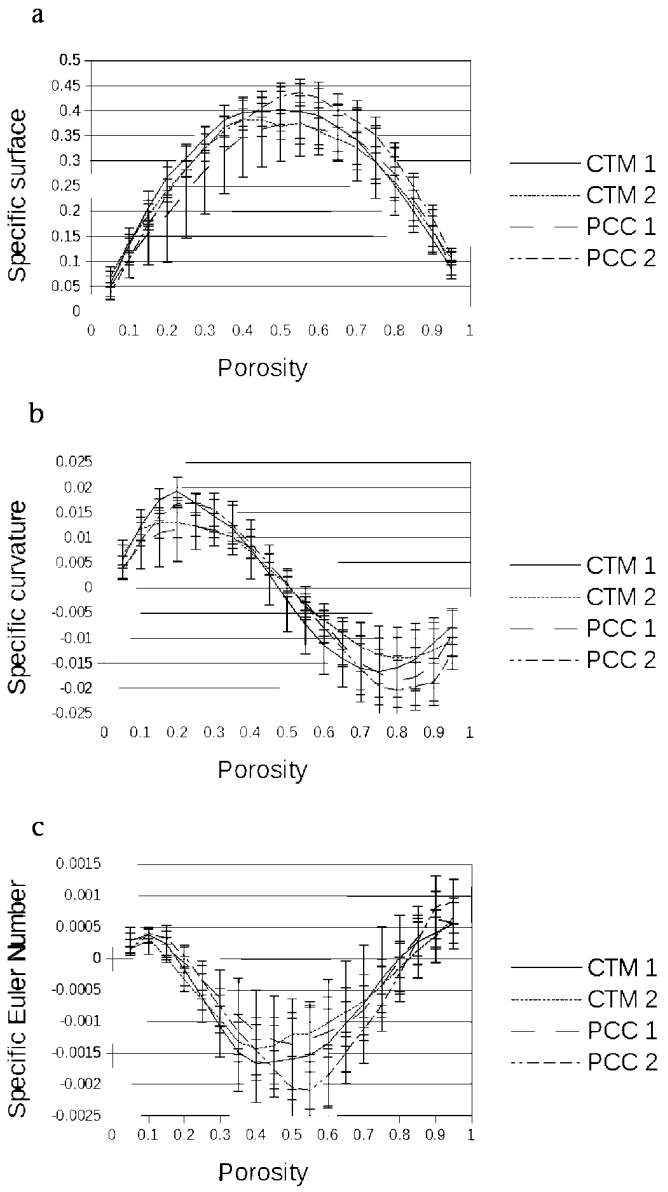

Fig. 5. Morphological functions built over Minkowski functionals for evolution of geometrical features when threshold varies as functions of image porosity.

we built the inverse function $r(\phi)$. Let us recall again that $\phi(r)$ is not the soil porosity of the sample but the volume fraction of voxels of the eroded and dilated pore space P_r of the cube c_i. Then, we obtained Minkowski densities as function of porosity for each cube c_i (Fig. 7)

$$\overline{S}_r(\phi)=S\left[P_{r(\phi)}\right]/V(c_i)\,,\ \overline{M}_r(\phi)=M\left[P_{r(\phi)}\right]/V(c_i)\,,$$

$$\overline{\chi}_r(\phi)=\chi\left[P_{r(\phi)}\right]/V(c_i)\,.$$

These morphological functions accounted for the evolutions of the specific area, specific mean curvature, and specific connectivity of pore space P of cube c_i. In this way we investigated the change of these geometrical features when the radius of dilation and erosion varied as a function of volume fraction or image porosity.

To estimate these morphological functions, the edge effect problem (Serra, 1982) should be taken into account. The pore space P is observed through cube c_i that plays the role of a sampling window, and morphological transformations can only be performed inside this cube. As a consequence, any dilation and erosion will be affected by the proximity to the faces of the cube. Therefore, only the information a certain distance apart from the faces of the cube will be reliable when these transformations are performed. To avoid this problem, measurements of volume, surface, mean curvature, and connectivity should be modified. When dilation and erosion with a ball of radius r is performed, the Minkowski functionals should be estimated over a reduced cube obtained by shrinking the edges of the cube c_i by r pixels on both ends of the edges (Ohser and Mücklich, 2000).

In general the evolution of image porosity with threshold (Fig. 4) showed a steep pattern so that parts with low densities accumulated a great amount of volume in each sample. This behavior seemed more noticeable for samples from resident vegetation cover (PCC1 and 2) and produced longer left tails on samples from tillage soil (CTM1 and 2). This seemed to suggest that the samples with resident vegetation cover stored a larger amount of low density materials as voids or organic matter. These findings were in accordance with the increase of particulate organic C under resident vegetation cover at 5 to 15 cm soil depth in this experimental field (Peregrina et al., 2010).

The evolution of specific surface, mean curvature, and connectivity with threshold (Fig. 5) displayed a similar behavior as observed by Mecke (1996) and Roth et al. (2005). In these works only two-dimensional structures were considered, and the comparison should be limited. But it is worth noting the similarity of the evolution of the second functional (length in two dimensions and surface in three dimensions) and connectivity in both cases. In our case the evolution of these geometrical measurements (see Fig. 5a and 5c) displayed quite similar patterns for the soil samples investigated here. The variability of the five cubes values (as shown by standard deviation bars) limited the statistical significance of the differences observed at this stage of the investigation. Specific surfaces (Fig. 5a) increased with porosity until it reached approximately 50% and then diminished having a parabola-like shape: small "grains" of voids grew, producing the growth of the boundary surface until they overlapped and began to connect to one another, thereby reducing the boundary surface. The evolution of specific mean curvatures (Fig. 5b) followed a sinusoidal curve that attained its maximum around 25% of porosity to go down to zero at about 50% porosity, and then it reached its minimum at approximately

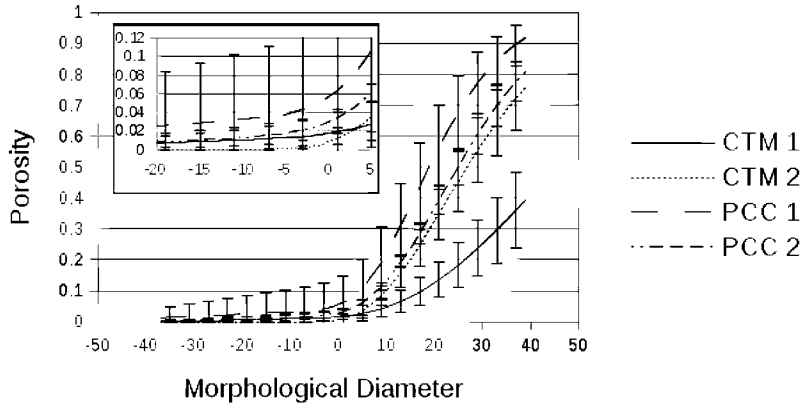

Fig. 6. Image porosity as function of dilation and erosion. The inset shows the graph of this function for negative values, that is, erosions.

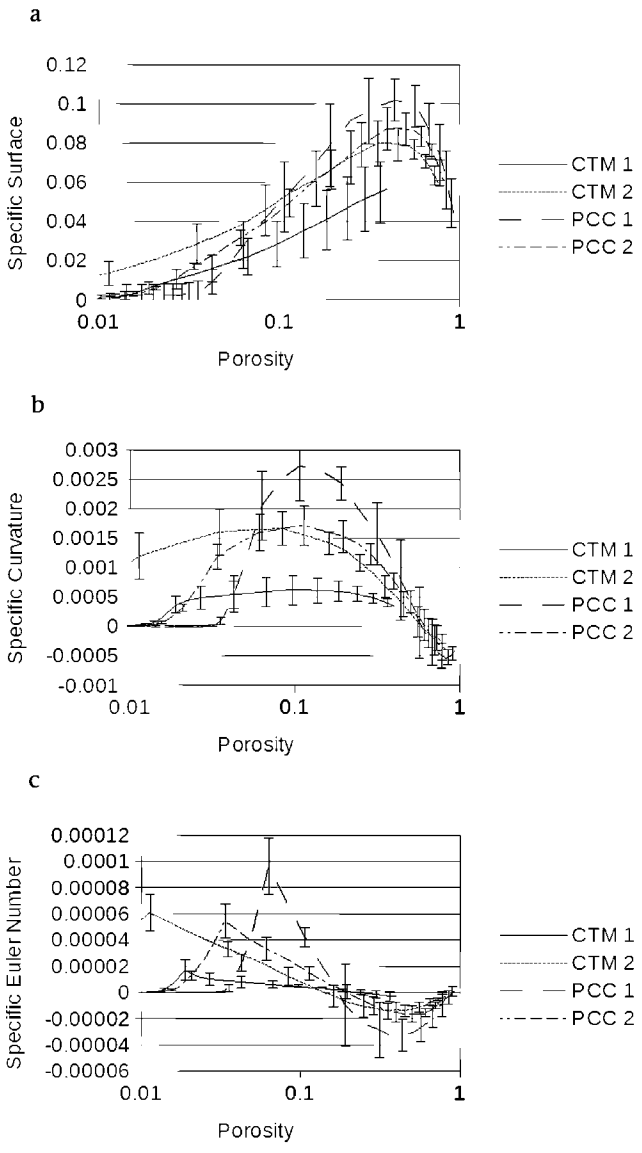

Fig. 7. Morphological functions built over Minkowski functionals for the evolution of geometrical features as a function of erosion and dilation as functions of image porosity.

75% porosity. At low threshold levels, image porosity was made of convex "grains" (i.e., they had positive mean curvature), but when they expanded as the threshold increased, these "grains" began to touch one another, producing concave parts or hollows and tunnels of soil materials through the pore space. These tunnels first compensated the convex parts as the specific mean curvature attained zero; afterward, curvature reached the minimum at a negative value, and then the complexity of the structure began to diminish and fill the entire cube. Specific Euler numbers (Fig. 5c) had a basin profile-like shape. As a reminder, the Euler number is evaluated as the number of connected components of the object of interest minus its tunnels plus its cavities. As we are dealing with images of a natural soil, we may assume that there are no soil materials completely surrounded by voids, and as a consequence, the Euler number corresponds to the number of connected components of the pores space minus the number of tunnels through the pore space at each grayscale level. Taking into account the evolution of curvature and connectivity simultaneously, Fig. 5b and 5c suggest that negative values of the mean curvature should be related to the appearance of soil materials tunnels (actually bridges) through soil voids as the threshold increases.

The evolution of image porosity with dilation and erosion is depicted in Fig. 6. Samples with resident vegetation cover stored a greater amount of volume fraction at any diameter of the balls used to erode (negative values of the diameter) and dilate (positives values of the diameter) the pore space. This was consistent with the evolution of image porosity with threshold. Let us note that the diameters considered in the erosions and dilations did not allow attaining a porosity one in all samples. Binary images obtained when the threshold were selected with the method of modes conferred more porosity to samples with resident vegetation cover. This was consistent with results reported by Peregrina et al. (2010) as noted before: these samples had more porosity and organic matter than samples from tillage. It could be the effect of soil quality improvement by the use of permanent covers crops in the vineyard. Peregrina et al. (2010) observed also the formation

of newly stable aggregates under resident vegetation cover that should be connected with the porosity increase as compared with soil under conventional tillage.

Figure 7 displays the evolution of geometric measurements with erosion and dilation diameter variation as a function of porosity with logarithmic scale. The evolution of Minkowski functional as shown in Fig. 7 kept a certain similarity with the evolution of Minkowski features with threshold that was more apparent with natural scale (not shown) than with logarithmic scale. The logarithmic scale was chosen to enhance differences between pore structures of the two types of considered samples. Differences between samples with resident vegetation cover and samples with tillage were noticeable even if in most cases they were not statistically significant. They suggested that resident vegetation cover tends to generate a pore space with more specific surface (Fig. 7a). Specific mean curvature evolution (Fig. 7b) seemed to indicate that at low porosities (around 10%) resident vegetation cover produced mostly convex pores as compared with samples from tillage soil, but at high porosity they displayed a more complex structure as it showed the lower negatives values of curvature as compared to tillage soil. Sample CTM2 had a different behavior for porosities lower than 10% that we will examine below. Finally, specific connectivity evolution (Fig. 7c) also displayed more variation when samples were collected on soil with resident vegetation cover. It suggested a richer structure of pore space generated by resident vegetation cover where a great amount of disconnected voids appeared at low porosities and a highly connected pore space with a high density of soil materials tunneled through it at high porosities.

Let us examine here the distinct behavior of sample CTM2. This was the sample with the lowest porosity when the pore space was eroded (Fig. 6 inset). Nevertheless, at low porosity CTM2 had a greater amount of specific surface (Fig. 7a), specific mean curvature (Fig. 7b), and specific connectivity as compared with the other samples. If the CTM2 specific surface was larger than in the other samples, then CTM2 porosity should have displayed an intricate boundary or should have been made of small "grains." The high positive values of the specific connectivity (Fig. 7c) for low porosities suggested that the CTM2 pore structure contained a great amount of small features as the number of small voids (i.e., connected components) surpasses the number of soil materials that tunneled through them; therefore, high values of the specific mean curvature from these small features of the CTM2 pore space should be explained by the regularity of the surface that enclosed them. Let us recall that convex objects have positive mean curvature. It will be negative when concave parts dominate over convex ones on the boundary surface of a three-dimensional object. Sample CTM1 followed the same trend at the lowest porosity, but in this case it was less pronounced. Therefore, at low porosities smaller than 10%, samples from tillage displayed a great amount of small and regular features as compared with samples from resident vegetation cover. When the volume fraction or porosity went beyond 10%, resident vegetation cover displayed a distinct pattern characterized by a highly connected structure as a consequence of the high values of specific surface, mean curvature close to zero, and negative low values of specific connectivity. These results suggest that evolution of morphological features with dilation and erosion is more informative as an indicator of structure than moving threshold for cultivated soil in a Mediterranean vineyard.

It is worth noting that the evolution of these geometric features was similar to that in synthetic models built with Poisson distributed objects as cubes or overlapping oblate and prolate spheroids (Arns et al., 2004). Arns et al. (2004) made use of morphological functions based on dilation and erosion to test the accuracy of these Poisson random models to replicate the morphology of Fontainebleau sandstone. They found that these models could mimic experimental data, but none stood out as being "brilliant." In that respect, it is interesting to note here that Lehmann (2005) and Schlüter and Vogel (2011) performed a more broad investigation of geometrical features of porous media and its impact on transport and flow phenomena, and they arrived at the same conclusion: measurements other than ones based on Minkowski functionals are needed to understand the effect of pore space geometry on flow and transport phenomena. Lehmann (2005) and Schlüter and Vogel (2011) suggested that chord length distribution should be the candidate for additional measurements as it accounts for correlations over larger distances.

Conclusions

We introduced the following elements of mathematical morphology: the morphological transformations of erosion and dilation and two morphological functions built over Minkowski functionals. We have shown how to apply them to the morphological characterization of the pore space from natural soils through the basic geometrical features that Minkowski functionals represent. We observed that morphological functions of the threshold display features similar to those observed in previous work of Mecke (1996) and Roth et al. (2005). Morphological functions of dilation and erosion seem to discriminate between two a pore structures in a Mediterranean vineyard soil where two different soil management were applied: CTM and PCC of resident vegetation.

Further investigations are needed to encompass a wider range of soil management for understanding the role of morphological parameters in discrimination of a priori different natural soil structures and for determining accurate models to mimic pore structure of natural soils.

Acknowledgments

This work was partially supported by Plan Nacional de Investigación Científica, Desarrollo e Investigación Tecnológica (I+D+I) under ref. AGL2011/251675 and DGUI (Comunidad de Madrid) and UPM under ref. QM100245066.We thank the staff of the Servicio de Investigación y Desarrollo Tecnológico Agroalimentario (Gobierno La Rioja) for providing the experimental plots and helping with the field work and Thomas Redenbach at Fraunhofer ITWM where soil columns were imaged.

References

Arns, C.H., M.A. Knackstedt, and K.R. Mecke. 2002. Characterizing the morphology of disordered materials. In: K.R. Mecke and D. Stoyan, editors, Morphology of condensed matter. LNP 600. Springer Verlag, Berlin, Germany. p. 37–74.

Arns, C.H., M.A. Knackstedt, and K.R. Mecke. 2004. Characterization of irregular spatial structures by parallel sets and integral geometric measures. Colloids Surf. A Physicochem. Eng. Asp. 241:351–372. doi:10.1016/j.colsurfa.2004.04.034

Banhart, J., editor. 2008. Advanced tomographic methods in materials research and engineering. Oxford Univ. Press, Oxford, UK.

Brewer, R. 1964. Fabric and mineral analysis of soils. John Wiley & Sons, New York.

Dullien, F.A.L. 1992. Porous media: Fluid transport and pore structure. 2nd ed. Academic Press, San Diego, CA.

Horgan, G.W. 1998. Mathematical morphology for analyzing soil structure from images. Eur. J. Soil Sci. 49:161–173. doi:10.1046/j.1365-2389.1998.00160.x

Iassonov, P., T. Gebregenus, and M. Tuller. 2009. Segmentation of X-Ray CT images of porous materials: A crucial step for characterization and quantitative analysis of pore structures. Water Resour. Res. 45:W09415. doi:10.1029/2009WR008087

Klette, R., and A. Rosenfeld. 2004. Digital geometry. Geometric methods for digital picture analysis. Morgan Kaufman Publ., San Francisco, CA.

Lehmann, P. 2005. Pore structures: Measurement, characterization and relevance for flow and transport in soils. Proc. Appl. Math. Mech. 5:39–42. doi:10.1002/pamm.200510011

Lehmann, P., M. Berchtold, B. Ahrenholz, J. Tölke, A. Kaestner, M. Krafczyk, H. Flühler, and H.R. Künsch. 2008. Impact of geometrical properties on permeability and fluid phase distribution in porous media. Adv. Water Resour. 31:1188–1204. doi:10.1016/j.advwatres.2008.01.019

Lehmann, P., P. Wyss, A. Flisch, E. Lehmann, P. Vontobel, M. Krafczyk, A. Kaestner, F. Beckmann, A. Gygi, and H. Flühler. 2006. Tomographical imaging and mathematical description of porous media used for the prediction of fluid distribution. Vadose Zone J. 5:80–97. doi:10.2136/vzj2004.0177

Matheron, G. 1975. Random sets and integral geometry. John Wiley & Sons, New York.

Mecke, K.R. 1996. Morphological characterization of patterns in reaction-diffusion systems. Phys. Rev. E Stat. Phys. Plasmas Fluids Relat. Interdiscip. Topics 53(5):4794–4800. doi:10.1103/PhysRevE.53.4794

Mecke, K.R. 1998. Integral geometry and statistical physics. Int. J. Mod. Phys. B 12(9):861–899. doi:10.1142/S0217979298000491

Mecke, K.R. 2002. The shape of parallel surfaces: Porous media, fluctuating interfaces and complex fluids. Phys. A 314:655–662. doi:10.1016/S0378-4371(02)01047-6

Mecke, K., and C.H. Arns. 2005. Fluids in porous media: A morphometric approach. J. Phys. Condens. Matter 17:S503–S534. doi:10.1088/0953-8984/17/9/014

Mecke, K.R., and D. Stoyan, editors. 2000. Statistical physics and spatial statistics. The art of analyzing and modeling spatial structures and pattern formation. LNP 554. Springer Verlag, Berlin, Germany.

Mecke, K.R., and D. Stoyan, editors. 2002. Morphology of condensed matter. LNP 600. Springer Verlag, Berlin, Germany.

Mees, F., R. Swennen, M. van Geet, and P. Jacobs, editors. 2003. Applications of X-ray computed tomography in geosciences. Spec. Publ. 215. Geol. Soc. London, London, UK.

Michielsen, K., and H. De Raedt. 2001. Integral–geometry morphological image analysis. Phys. Rep. 347:461–538. doi:10.1016/S0370-1573(00)00106-X

Moran, C.J., A.B. McBratney, and A.J. Koppi. 1989. A rapid method for analysis of soil macropore structure. I. Specimen preparation and digital binary image production. Soil Sci. Soc. Am. J. 53:921–928. doi:10.2136/sssaj1989.03615995005300030048x

Moran, C.J., A.B. McBratney, and A.J. Koppi. 1990. A rapid method for analysis of soil macropore structure. II. Stereological model, statistical analysis, and interpretation. Soil Sci. Soc. Am. J. 54:509–515. doi:10.2136/sssaj1990.03615995005400020037

Ohser, J., and F. Mücklich. 2000. Statistical analysis of microstructure in materials sciences. John Wiley & Sons, Chichester, UK.

Peregrina, F., C. Larrieta, S. Ibáñez, and E. García-Escudero. 2010. Labile organic matter, aggregates, and stratification ratios in a semiarid vineyard with cover crops. Soil Sci. Soc. Am. J. 74(6):2120–2130. doi:10.2136/sssaj2010.0081

Perret, J., S.O. Prasher, A. Kantzas, and C. Langford. 1999. Three-dimensional quantification of macropore networks in undisturbed soil cores. Soil Sci. Soc. Am. J. 63:1530–1543. doi:10.2136/sssaj1999.6361530x

Peyton, R.L., C.J. Gantzer, S.H. Anderson, B.A. Haeffner, and P. Pfeifer. 1994. Fractal dimension to describe soil macropore structure using X-ray computed tomography. Water Resour. Res. 30:691–700. doi:10.1029/93WR02343

Pierret, A., Y. Capowiez, L. Belzunces, and C.J. Moran. 2002. 3D reconstruction and quantifi cation of macropores using x-ray computed tomography and image analysis. Geoderma 106:247–271. doi:10.1016/S0016-7061(01)00127-6

Roth, R., J. Boike, and H.J. Vogel. 2005. Quantifying permafrost patterns using Minkowski densities. Permafrost Periglacial Processes 16:277–290. doi:10.1002/ppp.531

Santaló, L.A. 1976. Integral geometry and geometric probability. Addison-Wesley, Reading, MA.

Serra, J. 1982. Image analysis and mathematical morphology. Academic Press, Orlando, FL.

Schlüter, S., and H.J. Vogel. 2011. On the reconstruction of structural and functional properties in random heterogeneous media. Adv. Water Resour. 34:314–325. doi:10.1016/j.advwatres.2010.12.004

Soille, P. 2002. Morphological textural analysis: An introduction. In: K.R. Mecke and D. Stoyan, editors. Morphology of condensed matter. LNP 600. Springer Verlag, Berlin, Germany. p. 215–237.

Sonka, M., V. Hlavac, and R. Boyle. 1998. Image processing, analysis, and machine vision. 2nd ed. PWS Publ., Pacific Grove, CA.

Sukop, M.C., and D.T. Thorne, Jr. 2007. Lattice Boltzmann modeling. An introduction for geoscientists and engineers. Springer Verlag, Berlin, Germany.

UNESCO. 1979. Map of the world distribution of arid regions. Map at scale 1:25,000,000 with explanatory note. UNESCO, Paris.

Vogel, H.J. 2002. Topological characterization of porous media. In: K.R. Mecke and D. Stoyan, editors, Morphology of condensed matter. LNP 600. Springer Verlag, Berlin, Germany. p. 75–92.

Vogel, H.J., H. Hoffmann, and K. Roth. 2005. Studies of crack dynamics in clay soil. I. Experimental methods, results, and morphological quantification. Geoderma 125:203–211. doi:10.1016/j.geoderma.2004.07.009

Vogel, H.J., and A. Kretzschmar. 1996. Topological characterization of pore space in soil—Sample preparation and digital image-processing. Geoderma 73:23–38. doi:10.1016/0016-7061(96)00043-2

Vogel, H.J., and K. Roth. 2001. Quantitative morphology and network representation of soil pore. Adv. Water Resour. 24:233–242. doi:10.1016/S0309-1708(00)00055-5

Vogel, J.H., U. Weller, and S. Schlüter. 2010. Quantification of soil structure based on Minkowski functions. Comput. Geosci. 36:1236–1245. doi:10.1016/j.cageo.2010.03.007

Wang, M., and Ch.H. Lai. 2009. A concise introduction to image processing using C++. Numerical Analysis and scientific computing series. Chapman & Hall/CRC, Boca Raton, FL.

Young, I.M., and J.W. Crawford. 2004. Interactions and self-organization in the soil-microbe complex. Science 304(5677):1634–1637. doi:10.1126/science.1097394